

8 *** Corresponding:** Shuming Jia (jiashm17@cardc.cn)



9 **Abstract.** Drifting snow storm is an important aeolian process that reshapes alpine
10 glaciers and polar ice shelves, and it may also affect the climate system and
11 hydrological cycle since flying snow particles exchange considerable mass and energy
12 with air flow. Prior studies have rarely considered the full-scale drifting snow storm in
13 the turbulent boundary layer, thus, the transportation feature of snow flow higher in
14 the air and its contribution are largely unknown. In this study, a large eddy simulation
15 is combined with a subgrid scale velocity model to simulate the atmospheric turbulent
16 boundary layer, and a Lagrangian particle tracking method is adopted to track the
17 trajectories of snow particles. A drifting snow storm that is hundreds of meters in
18 depth and exhibits obvious spatial structures is produced. The snow transport flux
19 profile at high altitude, previously not observed, is quite different from that near the
20 surface, thus, the extrapolated transport flux profile may largely underestimate the
21 total transport flux. At the same time, the development of a drifting snow storm
22 involves three typical stages, the rapid growth, the gentle growth and the equilibrium
23 stages, in which the large-scale updrafts and subgrid scale fluctuating velocities
24 basically dominate the first and second stage, respectively. This research provides an
25 effective way to get an insight into natural drifting snow storms.



26 **1 Introduction**

27 Snow, one type of solid precipitation, is an important sources of material to mountain
28 glaciers and polar ice sheets, which are widespread throughout high and cold regions
29 (Chang et al., 2016; Gordon and Taylor, 2009; Lehning et al., 2008). A common
30 natural phenomenon over snow cover is the drifting snow storm, which occurs when
31 the wind speed exceeds a critical value (Doorschot et al., 2004; Li and Pomeroy, 1997;
32 Sturm and Stuefer, 2013). Drifting snow can entrain loose snow particles on the bed
33 into the air, which may be further transported to high altitude by turbulent eddies
34 (King, 1990; Mann et al., 2000; Nemoto and Nishimura, 2004). Drifting snow clouds
35 typically can range in thickness from tens to thousands of meters (Mahesh et al., 2003;
36 Palm et al., 2011), which may not only affect people's daily life by reducing the
37 visibility and producing local accumulation (Gordon and Taylor, 2009; Mohamed et
38 al., 1998) , but also can influence the global climate system evolution by changing the
39 mass and energy balance of ice shelves (Cess and Yagai, 1991; Hanesiak and Wang,
40 2005; Hinzman et al., 2005; Lenaerts and Broeke, 2012).

41 Several field experiments on drifting snow storm have been performed (Bintanja,
42 2001; Budd, 1966; Dingle and Radok, 1961; Doorschot et al., 2004; Gallée et al.,
43 2013; Gordon and Taylor, 2009; Guyomarch et al., 2014; Kobayashi, 1978; Mann et
44 al., 2000; Nishimura and Nemoto, 2005; Nishimura et al., 2015; Pomeroy and Gray,
45 1990; Shuhei, 1985; Schmidt, 1982; Sturm and Stuefer, 2013) since the middle of the
46 last century. However, the measurements are commonly conducted near the surface,
47 thus, the drifting snow features at high altitude are unknown, and the impacts of these



48 features are difficult to assess. A thorough investigation documenting the evolution
49 process and structure of a full-scale drifting snow storm is essential to understand this
50 natural phenomenon and assess its impacts.

51 Drifting snow models, on the other hand, offer a panoramic view of the evolution
52 process of drifting snow and thus have become one of the most useful research
53 approaches. Many continuum medium models of drifting snow (Bintanja, 2000; Déry
54 and Yau, 1999; Schneiderbauer and Prokop, 2011; Uematsu et al., 1991; Vionnet et al.,
55 2013) have advanced the knowledge of natural drifting snow to a great extent.
56 However, a particle-tracking drifting snow model is still needed since the particle
57 characteristics and its motion require further investigation. Although a series of
58 particle tracking models (Huang et al., 2016; Huang and Shi, 2017; Huang and Wang,
59 2015; 2016; Nemoto and Nishimura, 2004; Zhang and Huang, 2008; Zwaafink et al.,
60 2014) have been established, these models have generally focused on the grain-bed
61 interactions and particle motions near the surface. Thus, a drifting snow model aimed
62 at producing a large-scale drifting snow storm in a turbulent boundary layer deserves
63 further exploration.

64 In this study, a drifting snow model in the atmospheric boundary layer that focuses
65 on the full-scale drifting snow storm is established. The wind field is solved using a
66 large eddy simulation for the purpose of generating a turbulent atmospheric boundary
67 layer. A subgrid scale (SGS) velocity is also considered to include the diffusive effect
68 of small scale turbulence. Finally, particle motion is calculated using a Lagrangian
69 particle tracking method. The large-scale drifting snow storm is produced and its



70 spatial structures and transport features are analyzed.

71 **2 Model and methods**

72 **2.1 Simulation of a turbulent atmospheric boundary layer**

73 The mesoscale atmosphere prediction pattern ARPS (Advanced Regional Prediction
 74 System, version 5.3.3) is adopted to simulate the turbulent atmospheric boundary
 75 layer, in which the filtered three-dimensional compressible non-hydrostatic
 76 Navier-Stokes equation is solved (Xue et al., 2001):

$$77 \quad \frac{\partial \rho}{\partial t} + \frac{\partial}{\partial x_i}(\rho \tilde{u}_i) = 0 \quad (1)$$

$$78 \quad \frac{\partial \rho \tilde{u}_i}{\partial t} + \frac{\partial \rho u_i \tilde{u}_j}{\partial x_j} = -\frac{\partial \tilde{p}^*}{\partial x_i} + B \delta_{i3} - \frac{\partial \tau_{ij}}{\partial x_j} \quad (2)$$

79 where ‘ \sim ’ represents variables that are filtered and the filtering scale is
 80 $\tilde{\Delta} = (\Delta x_1 \Delta x_2 \Delta x_3)^{1/3}$, in which Δx_i is the grid spacing along streamwise ($i=1$),
 81 spanwise ($i=2$) and vertical direction ($i=3$), respectively. u_i is the instantaneous
 82 wind speed component, and x_i is the position coordinate. t is time, δ_{ij} is the
 83 Kronecker delta, $B = -g \rho' / \rho$ is the buoyancy caused by the air density perturbation
 84 ρ' , and g is the acceleration due to gravity. $p^* = p' - \alpha \nabla \cdot (\rho \mathbf{u})$ contains the pressure
 85 perturbation term and damping term, where α is the damping coefficient and ∇ is
 86 the divergence. The subgrid stress τ_{ij} can be expressed as (Smagorinsky, 1963):

$$87 \quad \tau_{ij} = -2\nu_t \tilde{S}_{ij} = -2(C_s \tilde{\Delta})^2 |\tilde{S}| \tilde{S}_{ij} \quad (3)$$

88 where $\tilde{S}_{ij} = 0.5(\partial \tilde{u}_i / \partial x_j + \partial \tilde{u}_j / \partial x_i)$ is the strain rate tensor and $|\tilde{S}| = \sqrt{2\tilde{S}_{ij}\tilde{S}_{ij}}$, C_s
 89 is Smagorinsky coefficient that is determined locally by the dynamic Lagrangian
 90 model (Meneveau et al., 1996).



91 Considering the large grid spacing in simulating an atmospheric boundary layer
 92 (where the information about turbulent vortices smaller than the grid size is missing),
 93 the SGS velocity is also included. Namely, the local wind velocity $\tilde{u}_i(\vec{x}(t))$ is
 94 composed of a resolved Eulerian large-scale part $\tilde{u}_i(\vec{x}(t))$ (obtained from the linear
 95 weighting of surrounding grid points) and a fluctuating SGS contribution $u'_i(t)$. The
 96 SGS velocity can be calculated from the SGS stochastic model of Vinkovic et al.
 97 (2006):

$$98 \quad du'_i = \left(-\frac{1}{T_L} + \frac{1}{2\tilde{k}} \frac{d\tilde{k}}{dt} \right) u'_i dt + \sqrt{\frac{4\tilde{k}}{3T_L}} d\eta_i(t) \quad (4)$$

99 where $T_L = 4\tilde{k}/(3C_0\tilde{\varepsilon})$ is the Lagrangian correlation time scale. Here, C_0 is the
 100 Lagrangian constant, $\tilde{\varepsilon} = C_\varepsilon \tilde{k}^{3/2}/\tilde{\Delta}$ is the subgrid turbulence dissipation rate, C_ε is
 101 a constant, and $d\eta_i$ is the increment of a vector-valued Wiener process with zero
 102 mean and variance dt . \tilde{k} is the subgrid turbulent kinetic energy and can be obtained
 103 from the transport equation (Deardorff, 1980):

$$104 \quad \frac{\partial \tilde{k}}{\partial t} + \tilde{u}_j \frac{\partial \tilde{k}}{\partial x_j} = \frac{\nu_t}{3} \frac{g}{\theta_0} \frac{\partial \tilde{\theta}}{\partial x_3} + 2\nu_t \tilde{S}_{ij}^2 + 2 \frac{\partial}{\partial x_j} \left(\nu_t \frac{\partial \tilde{k}}{\partial x_j} \right) + \tilde{\varepsilon} \quad (5)$$

105 where θ is the potential temperature and θ_0 is the surface potential temperature.

106 2.2 Governing equation of particle motion

107 The trajectory of each snow particle is calculated using a Lagrangian particle tracking
 108 method. Since a snow particle has is almost 10^3 times more dense than air, airborne
 109 particles are assumed to process only gravity and fluid drag forces, and the governing
 110 equations of particle motion can be expressed as (Dupont et al., 2013; Huang and
 111 Wang, 2016; Vinkovic et al., 2006):



$$\frac{dx_{pi}}{dt} = u_{pi} \quad (6)$$

$$\frac{du_{pi}}{dt} = m_p \frac{V_{ri}}{T_p} f(Re_p) + \delta_{i3} g \quad (7)$$

where x_{pi} and u_{pi} are the position coordinate and velocity of the snow particle, respectively. m_p is the mass of the solid particle, V_r is the relative speed between the snow particle and air, and $T_p = \rho_p d_p^2 / 18 \rho \nu$ is the particle relaxation time, where ρ_p is the particle density, d_p is the particle diameter and $\nu = 1.5e-5$ is the dynamic viscosity of air. $f(Re_p)$ can be expressed as (Clift et al., 1978):

$$f(Re_p) = \begin{cases} 1 & (Re_p < 1) \\ 1 + 0.15 Re_p^{0.687} & (Re_p \geq 1) \end{cases} \quad (8)$$

where $Re_p = V_r d / \nu$ is the particle Reynolds number.

2.3 Initial conditions of snow particles

To generate a large-scale drifting snow storm, a steady-state snow saltation condition is set as the bottom boundary condition for particles. During drifting snow events, the sum of residual fluid shear stress τ_f and particle-borne shear stress τ_p should be equal to the total fluid shear stress τ , thus, the particle-borne stress can be expressed as:

$$\tau_p = \tau - \tau_f \quad (9)$$

Here, the residual fluid shear stress τ_f is set to be the threshold shear stress τ_{yf} of drifting snow, which can be read as (Clifton et al., 2006):

$$\tau_{yf} = A^2 g d (\rho_p - \rho) \quad (10)$$

in which $A = 0.2$ is a constant, g is the gravity acceleration and d is the mean diameter of the snow particles.



At the same time, the particle-borne shear stress at the surface can be calculated from the particle trajectories as (Nemoto and Nishimura, 2004):

$$\tau_p = \sum_{i=1}^{n_{\downarrow}} m_i u_{pi\downarrow} - \sum_{i=1}^{n_{\uparrow}} m_i u_{pi\uparrow} \quad (11)$$

where m_i is the mass of particle and $u_{pi\downarrow}$ and $u_{pi\uparrow}$ are the horizontal speeds of impact and lift-off particles, respectively. n_{\downarrow} and n_{\uparrow} are the particle number per unit area in unit time of impact and lift-off grains, respectively, which should be equivalent in steady-state saltation. Thus, the number of lift-off particles per unit area is:

$$n_{\uparrow} = n_{\downarrow} = \frac{\tau_p}{\langle m_i \rangle (1 - \langle e_h \rangle) \langle u_{pi\downarrow} \rangle} \quad (12)$$

in which $\langle \rangle$ indicates the overall average, and e_h is the horizontal restitution coefficient of snow particle. According to Sugiura and Maeno (2000), the mean horizontal restitution coefficient can be expressed as:

$$\langle e_h \rangle = \begin{cases} 0.48 \theta_i^{0.01} & v_i \leq 1.27 \text{ ms}^{-1} \\ 0.48 \left(\frac{v_i}{1.27} \right)^{-\log\left(\frac{v_i}{1.27}\right)} \theta_i^{0.01} & v_i > 1.27 \text{ ms}^{-1} \end{cases} \quad (13)$$

where θ_i and v_i are the impact velocity and angle, respectively. Here, θ_i has a mean value of approximately 10° (Sugiura and Maeno, 2000), and $\langle v_i \rangle$ is set to be the threshold of impact velocity, which is determined by setting ejection number $n_e = 0.51 v_i^{0.6} \theta_i^{0.16}$ equal to 1. In this way, the mean horizontal velocity of impact particles can be obtained through $\langle u_{pi\downarrow} \rangle = \langle v_i \rangle \cos \langle \theta_i \rangle$.

Then, the velocities of lift-off particles can be obtained from the restitution coefficient of snow. The horizontal restitution coefficient obeys the normal



distribution with a mean value given in Eq. 13, and a standard variance as follow
 (Sugiura and Maeno, 2000):

$$\sigma^2 = \begin{cases} 0.07\theta_i^{-0.06} & v_i \leq 0.52 \text{ ms}^{-1} \\ 0.07\left(\frac{v_i}{0.52}\right)^{-\log(\frac{v_i}{0.52})}\theta_i^{-0.06} & v_i > 0.52 \text{ ms}^{-1} \end{cases} \quad (14)$$

On the other hand, the vertical restitution coefficient can be described by a two
 parameter gamma function (see Eq. 17), in which the parameter α and β can be
 expressed as (Sugiura and Maeno, 2000):

$$\alpha = \begin{cases} 1.22\theta_i^{0.47} & v_i \geq 0.84 \text{ ms}^{-1} \\ 1.22\left(\frac{v_i}{0.84}\right)^{\log(\frac{v_i}{0.84})}\theta_i^{0.47} & 0.84 < v_i \leq 1.23 \text{ ms}^{-1} \\ 1.22\left(\frac{v_i}{0.84}\right)^{\log(\frac{v_i}{0.84})}\left(\frac{v_i}{1.23}\right)^{-2\log(\frac{v_i}{1.23})}\theta_i^{0.47} & v_i \geq 1.23 \text{ ms}^{-1} \end{cases} \quad (15)$$

$$\beta = \begin{cases} 12.85\theta_i^{-1.41} & v_i \geq 0.84 \text{ ms}^{-1} \\ 12.85\left(\frac{v_i}{0.84}\right)^{-\log(\frac{v_i}{0.84})}\theta_i^{-1.41} & 0.84 < v_i \leq 1.23 \text{ ms}^{-1} \\ 12.85\left(\frac{v_i}{0.84}\right)^{-\log(\frac{v_i}{0.84})}\left(\frac{v_i}{1.23}\right)^{\log(\frac{v_i}{1.23})}\theta_i^{-1.41} & v_i \geq 1.23 \text{ ms}^{-1} \end{cases} \quad (16)$$

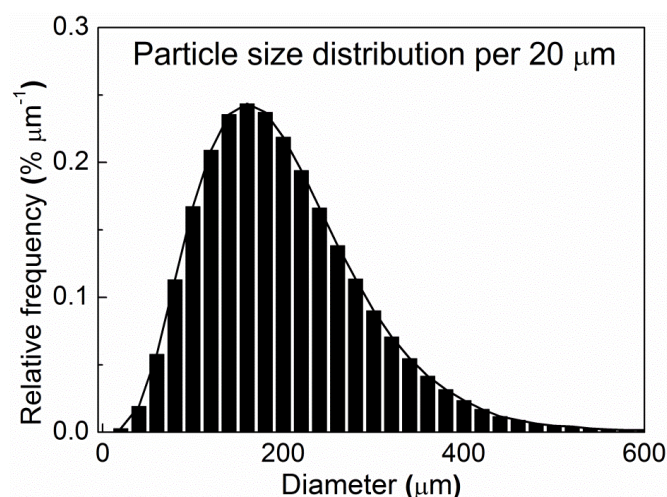
2.4 Simulation details

The computational domain is $1000 \times 500 \times 1000$ m, with a uniform horizontal grid
 size of 5 m adopted to solve finer vortex structure in the atmospheric boundary layer.
 The mean grid size in the vertical direction is 20 m, with a grid refinement algorithm
 adopted near the surface (the finest grid size is 1 m). Periodic boundaries are used
 along streamwise and spanwise dimensions, and the bottom is set as a grid wall. The
 top is set as an open radiation boundary with a Rayleigh damping layer that is 250 m
 in depth.



169 The atmosphere is neutral with an initial potential temperature of 300K, and an
 170 initial relative humidity of 90%. The initial wind profile is logarithmic with a surface
 171 roughness of 0.1m (Doorschot et al., 2004). Atmospheric turbulence is induced by
 172 random initial potential temperature perturbations at the first-level grid level with a
 173 maximum magnitude of 0.5K, and is sustained by a constant heat flux at the bottom.
 174 The constant heat flux is 50 Wm^{-2} according to the observation of Pomeroy and
 175 Essery (1999).

176 For particles, periodic boundary conditions are also used at lateral boundaries, and
 177 a rebound boundary condition without energy loss is adopted at the model top. The
 178 bottom boundary condition for particles is given in Sect. 2.3, and is updated every 0.5
 179 s. Additionally, each particle represents one particle parcel for the purpose of reducing
 180 computational complexity.



181
 182 **Figure 1.** Size distribution of lift-off snow particles in this simulation.

183 The size distribution of lift-off particles in drifting snow can be well described by
 184 the two-parameter gamma function (Budd, 1966; Gordon and Taylor, 2009;



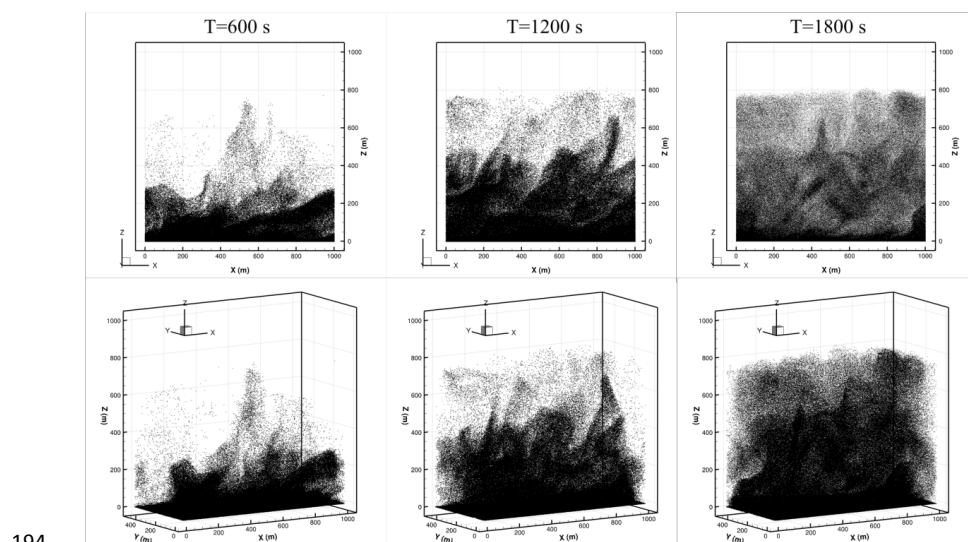
185 Nishimura and Nemoto, 2005; Schmidt, 1982):

$$186 \quad f(d) = \frac{d^{\alpha-1}}{\beta^\alpha \Gamma(\alpha)} \exp\left(-\frac{\beta}{d}\right) \quad (17)$$

187 where d is the particle diameter, and α and β are the shape and scale parameter of
 188 the distribution, respectively. In this simulation, the diameters of lift-off snow
 189 particles are given randomly from a gamma function with the parameters of $\alpha = 4$
 190 and $\beta = 50$, as shown in Fig. 1, which is also consistent with observed particle size
 191 distributions (Nishimura and Nemoto, 2005; Schmidt, 1982).

192 3 Results and discussions

193 3.1 Model validation



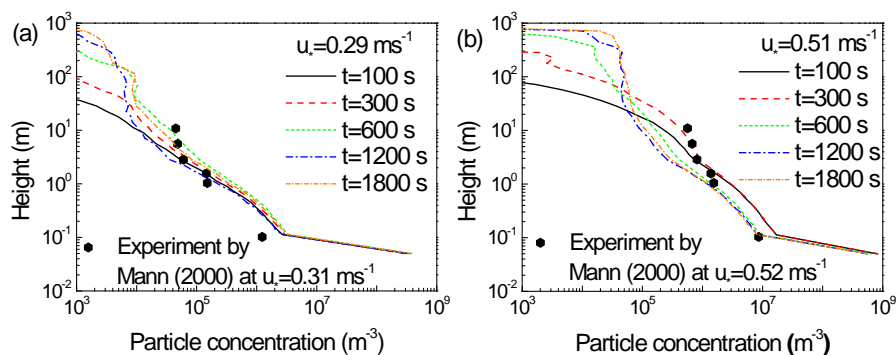
194
 195 **Figure 2.** Drifting snow storm at different moments under the friction velocity of 0.29
 196 ms^{-1} .

197 When drifting snow occurs in the atmospheric boundary layer, updrafts and
 198 turbulence fluctuations can send snow particles to high altitude, forming a fully
 199 developed drifting snow storm. Fig. 2 shows the drifting snow storm in the



200 atmospheric boundary layer at different moments, in which the friction velocity is
 201 $u_* = 0.29 \text{ ms}^{-1}$ and dark spots represent snow particles. It can be seen that drifting
 202 snow storm experiences an evolution process from near the surface to high altitudes,
 203 which induces the fact that particle concentration decreases along increasing height.
 204 The high concentrations of drifting snow cloud are generally below 500 m, though
 205 snow particles may reach up to approximately 800 m under this condition. This is also
 206 consistent with observations (Mahesh et al., 2003; Palm et al., 2011).

207 Since a drifting snow storm exhibits a different structure from bottom to top, the
 208 evolution of particle number density profile in the drifting snow storm is shown in Fig.
 209 3, which is also compared with measurements of Mann et al. (2000). From this figure,
 210 the thickness of the drifting snow layer obviously increases with time, and almost
 211 approaches its steady state after 1200 s. At the same time, the particle number density
 212 basically decreases with height, which is consistent with the measurements of Mann
 213 et al. (2000) at various friction velocities. The predicted particle number density at the
 214 surface is much larger than at higher altitude and observations, mainly because the
 215 saltating particles are also included.

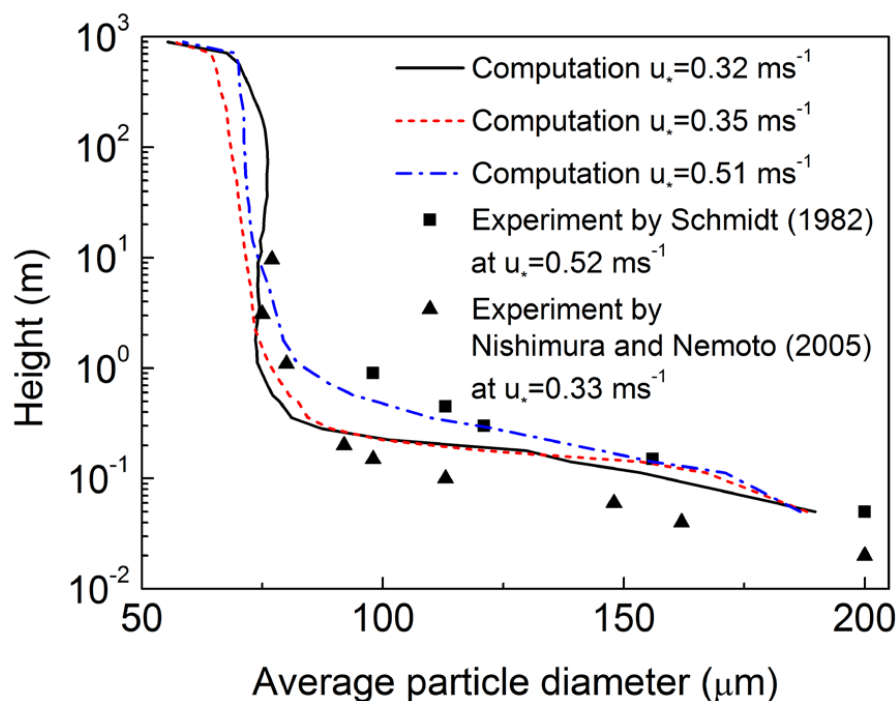


217 **Figure 3.** Evolution of particle number density under various friction velocities (a)



218 0.29 ms^{-1} and (b) 0.51 ms^{-1} .

219 Generally, smaller particles are more likely to be transported higher in the air. Fig.
 220 4 shows the variation of modeled average particle diameter versus height, which is
 221 also compared with various field measurements (Nishimura and Nemoto, 2005;
 222 Schmidt, 1982). Similar to the field observations, the average particle size basically
 223 decreases with height at lower altitude but is almost constant above 1 m. The average
 224 particle diameter is approximately $75 \mu\text{m}$ ranging from one meter to hundreds of
 225 meters in height, which is also consistent with the measurements of K Nishimura and
 226 Nemoto (2005).

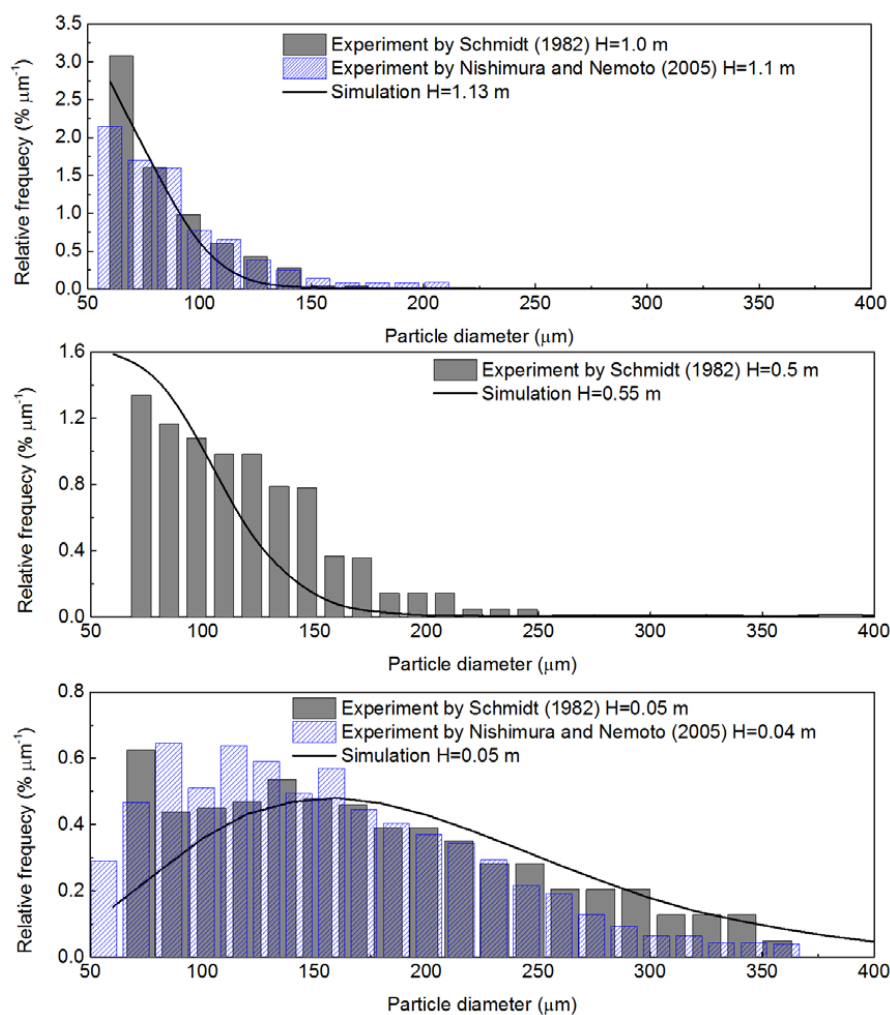


227
 228 **Figure 4.** Variation of average particle diameter versus height.

229 Then, the particle size distributions at various heights are also compared with
 230 experiment results. As shown in Fig. 5, the heights are 0.05 m, 0.5 m and 1 m. The



231 modeled particle size distributions at various heights are consistent with the
 232 measurements (Nishimura and Nemoto, 2005; Schmidt, 1982). Therefore, the
 233 established model is able to produce a large-scale drifting snow storm.



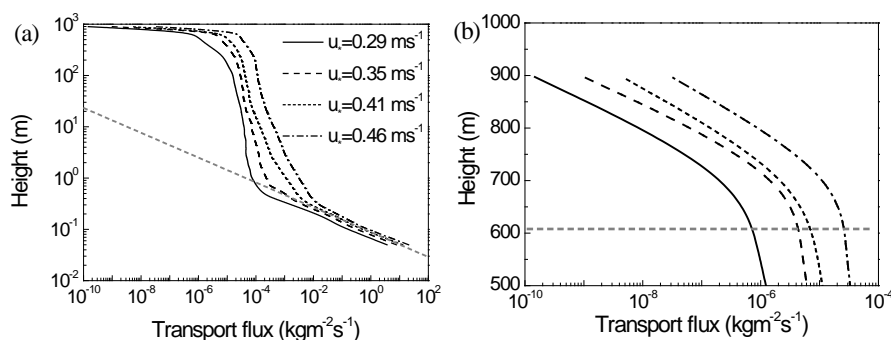
234
 235 **Figure 5.** Particle size distribution at various heights.

236 3.2 Snow transport flux

237 The snow transport flux is of great importance to predict the mass and energy
 238 balances of ice sheets. The total transport flux can be obtained from vertical



239 integration of the snow transport flux profile.

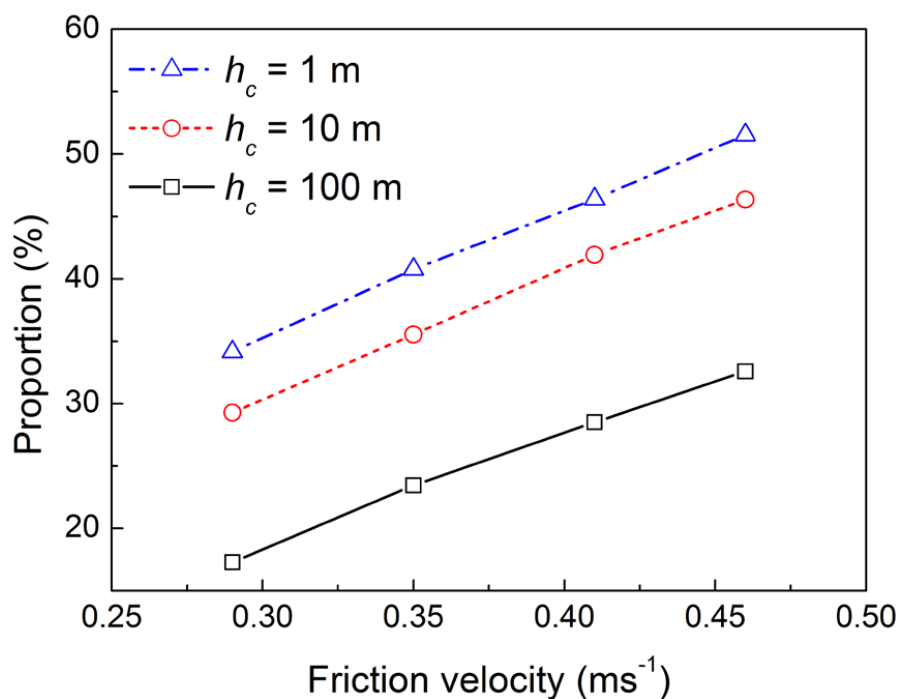


240

241 **Figure 6.** Variations of snow transport flux versus height.

242 The profiles of snow transport rate, per unit area, per unit time, under various
 243 friction velocities are shown in Fig. 6(a). It can be seen that the transport flux
 244 undergoes a sharp decrease with height at lower altitude (e.g., below 1.0 m), however,
 245 the transport flux tends to decrease rather gentle until almost the top of the drifting
 246 snow storm, as shown in Fig. 6(b), probably due to the large-scale turbulent motion
 247 and increasing wind speed with height. In other words, the suspension flux of drifting
 248 snow at higher altitudes, previously not observed, may be much larger than we
 249 previously thought.

250 In previous studies, the transport flux profile is commonly described using an
 251 exponential decay form based on the extrapolation from measurements near the
 252 surface (Mann et al., 2000; Nishimura and Nemoto, 2005; Schmidt, 1982; 1984;
 253 Tabler, 1990), which may result in a considerable underestimate of the total transport
 254 flux. The proportions of suspension flux above a given height h_c (referred as Q_c) to
 255 the total suspension flux Q_s are shown in Fig. 7, in which snow particles below 0.1
 256 m are not calculated (Mann et al., 2000).



257
 258 **Figure 7.** Proportion of suspension flux above h_c to the total suspension flux under
 259 various friction velocities.

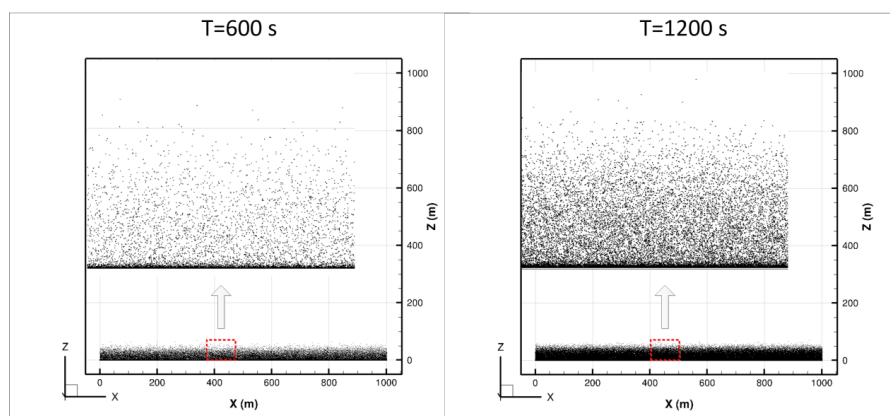
260 From Fig. 7, the contribution of Q_c to the total suspension flux is non-negligible
 261 under various h_c , the proportion of Q_c when $h_c=100 \text{ m}$ to the total suspension flux
 262 has exceeded 30% when the friction velocity is 0.46 ms^{-1} . At the same time, the
 263 proportion of Q_c to the total suspension flux increases with friction velocity but
 264 decreases with increasing h_c .

265 In this way, not only the snow transport flux, but also the sublimation of
 266 suspended snow particles should be reevaluated because the sublimation rate of snow
 267 particles higher in the air may be much larger than near the surface due to the lower
 268 air humidity and greater wind speed at higher altitude (Mann et al., 2000; Nishimura
 269 and Nemoto, 2005; Schmidt, 1982; 1984; Tabler, 1990).



270 3.3 Structures in a drifting snow storm

271 In a drifting snow storm, particles aggregate locally and produce special spatial
 272 structures (as shown in Fig. 2). These structures should be directly related to the
 273 turbulence structures present in the atmospheric boundary layer. Drifting snow storms
 274 without atmospheric turbulence are shown in Fig. 8. Compared with Fig. 2, drifting
 275 snow particles mainly travel at the near surface with a uniform spatial distribution
 276 when atmospheric turbulence is not included.

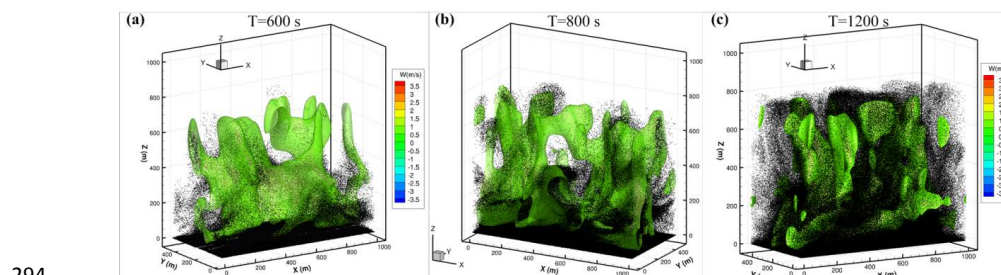


277
 278 **Figure 8.** Drifting snow storm without atmospheric turbulence under friction velocity
 279 of 0.35 ms^{-1} .

280 It is known that snow particles will become suspended if the local vertical wind
 281 speed exceeds the terminal velocity of particle. In a turbulent atmospheric boundary
 282 layer, there exists a large amount of turbulent structures with different scales and
 283 shapes. The vertical wind speed component of large-scale turbulence (namely, updraft)
 284 plays an important role in carrying snow particles to high altitude, while small scale
 285 turbulence (e.g., the SGS fluctuating velocity) tends to spread particles from high
 286 concentration zones to low concentration zones. As shown in Fig. 9(a), at the initial



287 period of a drifting snow storm, the structures in the drifting snow storm are
 288 consistent with large-scale updrafts, and snow particles are mainly located in the
 289 updraft. With the further development of the drifting snow storm, as shown in Fig.
 290 9(b), more snow particles are scattered around the updraft bubbles although high
 291 concentration particle clouds are still in the wind bubbles. When drifting snow storm
 292 approaches its saturated state, snow particle clouds are almost connected together with
 293 numerous high concentration zones inside.

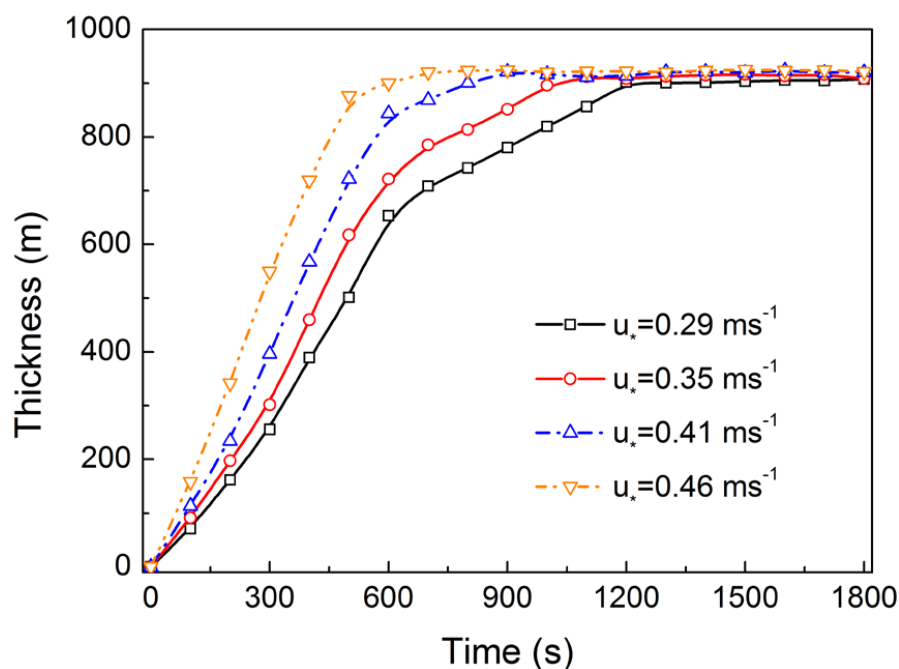


295 **Figure 9.** Evolution of drifting snow storm and vertical wind speed bubbles under
 296 friction velocity of 0.35 ms^{-1} , and wind bubbles are iso-surface of vertical wind speed
 297 with a value of 1.0 ms^{-1} .

298 The evolution of the depth of drifting snow storm can be divided into three typical
 299 stages. In sequence, these phases are the rapid growth phase, the gentle growth stage,
 300 and an equilibrium state, as shown in Fig. 10. Here, the depth of drifting snow storm
 301 refers to the average height of the topmost particle during this period (100 s). The
 302 rapid growth stage is mainly driven by large-scale turbulent motion, while the
 303 turbulent diffusion by the SGS fluctuating velocity is the main contributor to the
 304 gentle growth stage. The duration of second stage decreases with increasing friction
 305 velocity, which mainly comes from the stronger turbulent diffusion under larger



friction velocities.



307

308 **Figure 10.** Time evolutions of the thickness of drifting snow storm under various
 309 friction velocities.

310 At the same time, the time required for the drifting snow storm to reach its
 311 maximum thickness decreases with friction velocity, ranging from about 1200 s to
 312 approximate 600 s when the friction velocity increases from 0.29 ms^{-1} to 0.46 ms^{-1} .
 313 The thickness of saturated drifting snow storms is almost constant with a value
 314 approximately 900 m under different friction velocities, probably because the
 315 boundary layer depth as well as the surface heat flux are unchanged. Thus, the final
 316 thickness of a drifting snow storm should be largely dependent on the maximum
 317 height of atmospheric turbulences.

318 **4 Conclusion**



319 In this work, large-scale drifting snow storms are simulated in a large eddy simulation
320 combined with a particle tracking model that includes subgrid scale velocity
321 fluctuations. A typical drifting snow storm of several hundred meters in depth is
322 generated, and the structure of the particle cloud with different concentrations is also
323 produced. The transport flux profile has obviously different slopes near the surface
324 compared to higher altitudes, that is, transport flux at near surface decreases with
325 height sharply, but decreases more gentle at higher altitude. Previous studies may
326 largely underestimate the total transport during drifting snow storms.

327 At the same time, the evolution of the thickness of drifting snow storm generally
328 contains three stages. Drifting snow storm development generally begins with a rapid
329 growth stage driven by the large scale atmospheric turbulent motions, followed by a
330 gentle growth stage driven by the SGS fluctuating wind speed, before reaching an
331 equilibrium stage when the drifting snow approaches a saturated state. The second
332 stage becomes shorter with increasing friction velocity, mainly because stronger
333 turbulence under higher friction velocity enhances the turbulent diffusion of particles.

334

335 *Acknowledgements.* This work is supported by the CARDC Fundamental and Frontier
336 Technology Research Fund (FFTRF-2017-08, FFTRF-2017-09), the State Key
337 Program of National Natural Science Foundation of China (91325203), the National
338 Natural Science Foundation of China (11172118, 41371034), and the Innovative
339 Research Groups of the National Natural Science Foundation of China (11121202),
340 National Key Technologies R & D Program of China (2013BAC07B01).



References:

- Bintanja, R.: Snowdrift suspension and atmospheric turbulence. Part I: Theoretical background and model description, *Boundary-Layer Meteorology*, 95, 343-368, 2000.
- Bintanja, R.: Characteristics of snowdrift over a bare ice surface in Antarctica, *Journal of Geophysical Research Atmospheres*, 106, 9653-9659, 2001.
- Budd, W. F.: The Byrd snow drift project : outline and basic results, 71-134, American Geophysical Union, Washington, DC, 1966.
- Cess, R. D., and Yagai, I.: Interpretation of Snow-Climate Feedback as Produced by 17 General Circulation Models, *Science*, 253, 888-892, 1991.
- Chang, A. T. C., Foster, J. L., and Hall, D. K.: Nimbus-7 SMMR Derived Global Snow Cover Parameters, *Annals of Glaciology*, 9, 39-44, 2016.
- Clift, R., Grace, J. R., and Weber, M. E.: Bubbles, drops, and particles, 263-264, 1978.
- Clifton, A., Rüedi, J. D., and Lehning, M.: Snow saltation threshold measurements in a drifting-snow wind tunnel, *Journal of Glaciology*, 52, 585-596, 2006.
- Déry, S. J., and Yau, M. K.: A Bulk Blowing Snow Model, *Boundary-Layer Meteorology*, 93, 237-251, 1999.
- Deardorff, J. W.: Stratocumulus-capped mixed layers derived from a three-dimensional model, *Boundary-Layer Meteorology*, 18, 495-527, 1980.
- Dingle, W. R. J., and Radok, U.: Antarctic snow drift and mass transport, *Int. Assoc. Sci. Hydrol. Publ.*, 55, 77-81, 1961.
- Doorschot, J. J. J., Lehning, M., and Vrouwe, A.: Field measurements of snow-drift threshold and mass fluxes, and related model simulations, *Boundary-Layer Meteorology*, 113, 347-368, 2004.
- Dupont, S., Bergametti, G., Marticorena, B., and Simoëns, S.: Modeling saltation intermittency, *Journal of Geophysical Research Atmospheres*, 118, 7109-7128, 2013.
- Gallée, H., Trouvilliez, A., Agosta, C., Genthon, C., Favier, V., and Naaïm-Bouvet, F.: Transport of Snow by the Wind: A Comparison Between Observations in Adélie Land, Antarctica, and Simulations Made with the Regional Climate Model MAR, *Boundary-Layer Meteorology*, 146, 133-147, 2013.
- Gordon, M., and Taylor, P. A.: Measurements of blowing snow, Part I: Particle shape, size distribution, velocity, and number flux at Churchill, Manitoba, Canada, *Cold Regions Science & Technology*, 55, 63-74, 2009.
- Guyomarch, G., Goetz, D., Vionnet, V., Naaïmbouvet, F., and Deschatres, M.: Observation of Blowing Snow Events and Associated Avalanche Occurrences, 2014.
- Hanesiak, J. M., and Wang, X. L.: Adverse-Weather Trends in the Canadian Arctic, *Journal of Climate*, 18, 3140-3156, 2005.
- Hinzman, L. D., Bettez, N. D., Bolton, W. R., Chapin, F. S., Dyurgerov, M. B., Fastie, C. L., Griffith, B., Hollister, R. D., Hope, A., and Huntington, H. P.: Evidence and Implications of Recent Climate Change in Northern Alaska and Other Arctic Regions, *Climatic Change*, 72, 251-298, 2005.



- 384 Huang, N., Dai, X., and Zhang, J.: The impacts of moisture transport on drifting snow
385 sublimation in the saltation layer, *Atmospheric Chemistry & Physics*, 16,
386 7523-7529, 2016.
- 387 Huang, N., and Shi, G.: The significance of vertical moisture diffusion on drifting
388 Snow sublimation near snow surface, *Cryosphere*, 11, 3011-3021, 2017.
- 389 Huang, N., and Wang, Z. S.: A 3-D simulation of drifting snow in the turbulent
390 boundary layer, *Cryosphere Discussions*, 9, 301-331, 2015.
- 391 Huang, N., and Wang, Z. S.: The formation of snow streamers in the turbulent
392 atmosphere boundary layer, *Aeolian Research*, 23, 1-10, 2016.
- 393 King, J. C.: Some measurements of turbulence over an antarctic ice shelf, *Quarterly*
394 *Journal of the Royal Meteorological Society*, 116, 379-400, 1990.
- 395 Kobayashi, S.: Snow Transport by Katabatic Winds in Mizuho Camp Area, East
396 Antarctica, *Journal of the Meteorological Society of Japan*, 56, 130-139, 1978.
- 397 Lehning, M., Löwe, H., Ryser, M., and Raderschall, N.: Inhomogeneous precipitation
398 distribution and snow transport in steep terrain, *Water Resources Research*, 44,
399 278-284, 2008.
- 400 Lenaerts, J. T. M., and Broeke, M. R. V. D.: Modeling drifting snow in Antarctica
401 with a regional climate model: 2. Results, *Journal of Geophysical Research*
402 *Atmospheres*, 117, D05109, 2012.
- 403 Li, L., and Pomeroy, J. W.: Estimates of Threshold Wind Speeds for Snow Transport
404 Using Meteorological Data, *Journal of Applied Meteorology*, 36, 205-213, 1997.
- 405 Mahesh, A., Eager, R., Campbell, J. R., and Spinhirne, J. D.: Observations of blowing
406 snow at the South Pole, *Journal of Geophysical Research Atmospheres*, 108, 4707,
407 2003.
- 408 Mann, G. W., Anderson, P. S., and Mobbs, S. D.: Profile measurements of blowing
409 snow at Halley, Antarctica, *Journal of Geophysical Research Atmospheres*, 105,
410 24491-24508, 2000.
- 411 Meneveau, C., Lund, T. S., and Cabot, W. H.: A Lagrangian dynamic subgrid-scale
412 model of turbulence, *Journal of Fluid Mechanics*, 319, 353-385, 1996.
- 413 Mohamed, N., Florence, N. B., and Hugo, M.: Numerical simulation of drifting snow:
414 erosion and deposition models, *Annals of Glaciology*, 26, 191-196, 1998.
- 415 Nemoto, M., and Nishimura, K.: Numerical simulation of snow saltation and
416 suspension in a turbulent boundary layer, *Journal of Geophysical Research*
417 *Atmospheres*, 109, D18206, 2004.
- 418 Nishimura, K., and Nemoto, M.: Blowing snow at Mizuho station, Antarctica,
419 *Philosophical Transactions*, 363, 1647, 2005.
- 420 Nishimura, K., Yokoyama, C., Ito, Y., Nemoto, M., Naaim - Bouvet, F., Bellot, H.,
421 and Fujita, K.: Snow particle speeds in drifting snow, *Journal of Geophysical*
422 *Research Atmospheres*, 119, 9901-9913, 2015.
- 423 Palm, S. P., Yang, Y., Spinhirne, J. D., and Marshak, A.: Satellite remote sensing of
424 blowing snow properties over Antarctica, *Journal of Geophysical Research*
425 *Atmospheres*, 116, D16123, 2011.
- 426 Pomeroy, J. W., and Essery, R. L. H.: Turbulent fluxes during blowing snow: field
427 tests of model sublimation predictions, *Hydrological Processes*, 13, 2963-2975,



- 1999.
- Pomeroy, J. W., and Gray, D. M.: Saltation of snow, *Water Resources Research*, 26, 1583–1594, 1990.
- Sbuhei, T.: Characteristics of Drifting Snow at Mizuho Station, Antarctica, *Annals of Glaciology*, 6, 71-75, 1985.
- Schmidt, R. A.: Vertical profiles of wind speed, snow concentration, and humidity in blowing snow, *Boundary-Layer Meteorology*, 23, 223-246, 1982.
- Schmidt, R. A.: Transport rate of drifting snow and the mean wind speed profile, *Boundary-Layer Meteorology*, 34, 213-241, 1984.
- Schneiderbauer, S., and Prokop, A.: The atmospheric snow-transport model: SnowDrift3D, *Journal of Glaciology*, 57, 526-542, 2011.
- Smagorinsky, J.: GENERAL CIRCULATION EXPERIMENTS WITH THE PRIMITIVE EQUATIONS, *Monthly Weather Review*, 91, 99-164, 1963.
- Sturm, M., and Stuefer, S.: Wind-blown flux rates derived from drifts at arctic snow fences, *Journal of Glaciology*, 59, 21-34, 2013.
- Sugiura, K., and Maeno, N.: Wind-Tunnel Measurements Of Restitution Coefficients And Ejection Number Of Snow Particles In Drifting Snow: Determination Of Splash Functions, *Boundary-Layer Meteorology*, 95, 123-143, 2000.
- Tabler, R. D.: Estimating snow transport from wind speed record : Estimates versus measurements at Prudhoe Bay, paper presented at Alaska, Meeting of Western Snow Conference, 1990.
- Uematsu, T., Nakata, T., Takeuchi, K., Arisawa, Y., and Kaneda, Y.: Three-dimensional numerical simulation of snowdrift, *Cold Reg.sci.technol*, 20, 65-73, 1991.
- Vinkovic, I., Aguirre, C., Ayrault, M., and Simoëns, S.: Large-eddy Simulation of the Dispersion of Solid Particles in a Turbulent Boundary Layer, *Boundary-Layer Meteorology*, 121, 283-311, 2006.
- Vionnet, V., Martin, E., Masson, V., Guyomarc'H, G., Naaimbouvét, F., Prokop, A., Durand, Y., and Lac, C.: Simulation of wind-induced snow transport in alpine terrain using a fully coupled snowpack/atmosphere model, *Cryosphere Discussions*, 7, 2191-2245, 2013.
- Xue, M., Droegemeier, K. K., Wong, V., Shapiro, A., Brewster, K., Carr, F., Weber, D., Liu, Y., and Wang, D.: The Advanced Regional Prediction System (ARPS) – A multi-scale nonhydrostatic atmospheric simulation and prediction tool. Part II: Model physics and applications, *Meteorology & Atmospheric Physics*, 76, 143-165, 2001.
- Zhang, J., and Huang, N.: Simulation of Snow Drift and the Effects of Snow Particles on Wind, *Modelling & Simulation in Engineering*, 2008, 408075, 2008.
- Zwaafink, C. D. G., Diebold, M., Horender, S., Overney, J., Lieberherr, G., Parlange, M. B., and Lehning, M.: Modelling Small-Scale Drifting Snow with a Lagrangian Stochastic Model Based on Large-Eddy Simulations, *Boundary-Layer Meteorology*, 153, 117-139, 2014.